Conformational Dynamics of Partially Denatured Myoglobin Studied by Time-Resolved Electrospray Mass Spectrometry with Online Hydrogen−Deuterium Exchange[†,‡]

Douglas A. Simmons,[§] Stanley D. Dunn,[||] and Lars Konermann*[,§]

Departments of Chemistry and Biochemistry, The University of Western Ontario, London, Ontario N6A 5B7, Canada

Received February 19, 2003; Revised Manuscript Received March 26, 2003

ABSTRACT: This study demonstrates the use of electrospray mass spectrometry in conjunction with rapid online mixing ("time-resolved" ESI-MS) for monitoring protein conformational dynamics under equilibrium conditions. The hydrogen/deuterium exchange (HDX) kinetics of mildly denatured myoglobin (Mb) at pD 9.3, in the presence of 27% acetonitrile, were studied with millisecond time resolution. Analytical ultracentrifugation indicates that the average protein compactness under these solvent conditions is similar to that of native holomyoglobin (hMb). The mass spectrum shows protein ions in a wide array of charge and heme binding states, indicating the presence of multiple coexisting conformations. The experimental approach used allows the HDX kinetics of all of these species to be monitored separately. A combination of EX1 and EX2 behavior was observed for hMb ions in charge states 7+ to 9+, which predominantly represent nativelike hMb in solution. The EX1 kinetics are biphasic, indicating the presence of two protein populations that undergo conformational opening events with different rate constants. The EX2 kinetics observed for nativelike hMb are biphasic as well. All other charge and heme binding states represent non-native protein conformations that are involved in rapid interconversion processes, thus leading to monoexponential EX2 kinetics with a common rate constant. Burst phase labeling for these non-native proteins occurs at 125 sites. In contrast, the nativelike protein conformation shows burst phase labeling only for 88 sites. A kinetic model is developed which is based on the assumption of three distinct (un)-folding units in Mb. The model implies that the free energy landscape of the protein exhibits a major barrier. The crossing of this barrier is most likely associated with slow, cooperative opening/closing events of the heme binding pocket. Rapid conformational fluctuations on either side of the barrier give rise to the observed EX2 kinetics. Simulated HDX kinetics based on this model are in excellent agreement with the experimental data.

Many proteins are known to adopt partially folded conformations under mildly denaturing solvent conditions. Studies on these semidenatured states are of great importance for understanding a wide range of biological processes such as folding (*1*), amyloid formation (*2*), signal transduction (*3*), ligand binding (*4*), and protein transport across membranes (*5*). Recent work has shown that some proteins exhibit a significant degree of disorder, even under physiological conditions where they are biologically active (*6*), thus indicating that a highly ordered native structure is not necessarily a prerequisite for protein function (*4*, *7*).

Partially folded proteins are structurally heterogeneous ensembles, undergoing conformational fluctuations on time scales ranging from subnanoseconds to minutes. Experimental techniques capable of probing the dynamic nature of these species are crucial for obtaining a better understanding of their biophysical properties. One important approach in this area is based on NMR[1] spin relaxation measurements (*8*−*11*). Other powerful strategies involve the use of hydrogen−deuterium exchange (HDX) methods (*12*−*19*). HDX at sites that are sterically shielded from the solvent, and/or involved in stable hydrogen bonds, is mediated by structural fluctuations of the protein. The exchange kinetics observed in continuous labeling experiments are, therefore, related to the conformational dynamics of the polypeptide chain. Brief opening events mediating exchange may correspond to global or subglobal unfolding/refolding transitions or to local fluctuations (*13*, *20*, *21*). The exchange mechanism is commonly described by (*22*)

$$\mathrm{X{-}H_{closed}} \underset{k_{cl}}{\overset{k_{op}}{\rightleftharpoons}} \mathrm{X{-}H_{open}} \xrightarrow[D_2O]{k_{ch}} \text{exchanged} \qquad (1)$$

where k_{op} and k_{cl} are the rate constants for the opening and

[†] This work was supported by the Natural Sciences and Engineering Research Council of Canada (NSERC), the Canada Foundation for Innovation (CFI), The Ontario Ministry of Energy, Science, and Technology, and The University of Western Ontario.

[‡] We dedicate this work to the memory of Fritz Jähnig.

* To whom correspondence should be addressed. Telephone: (519) 661-2111 ext 86313. Fax: (519) 661-3022. E-mail: konerman@uwo.ca.

[§] Department of Chemistry.

[||] Department of Biochemistry.

[1] Abbreviations: 2hMb, myoglobin with two heme groups attached; aMb, apomyoglobin; aMb^{n+}, multiply protonated apomyoglobin ion $[aMb + nH]^{n+}$; aMb_N, "native" state of apomyoglobin; aMb_I, apomyoglobin folding intermediate; aMb_U, unfolded state of apomyoglobin; ESI, electrospray ionization; fwhm, full width at half-maximum; HDX, hydrogen−deuterium exchange; hMb, holomyoglobin; hMb_U, holomyoglobin in a non-native conformation; Mb, myoglobin; i.d., inner diameter; MS, mass spectrometry; NMR, nuclear magnetic resonance.

10.1021/bi034285e CCC: $25.00
Published on Web 04/25/2003

closing, respectively, of a particular exchangeable site. The chemical exchange rate constant, k_{ch}, represents the kinetics that would be expected for a fully unprotected hydrogen. For amide hydrogens, the k_{ch} value of any individual site depends on its neighboring amino acid side chains and on pD. Reference data obtained from dipeptide model compounds are available that allow the estimation of amide k_{ch} values for any set of solvent conditions (*12*, *13*, *23*, *24*). In the EX2 limit, characterized by $k_{cl} \gg k_{ch}$, the overall exchange rate constant, k_{ex}, is given by

$$k_{ex} = K_{op} k_{ch} \quad (2)$$

where $K_{op} = k_{op}/k_{cl}$ is the equilibrium constant of the opening reaction. Under EX2 conditions, most sites have to visit the open conformation many times before exchange occurs. Conversely, if $k_{ch} \gg k_{cl}$ (EX1 regime), complete labeling will occur with the first opening event, such that

$$k_{ex} = k_{op} \quad (3)$$

NMR spectroscopy has traditionally been the method of choice for analyzing proteins in isotopic labeling experiments. However, in recent years, the use of electrospray ionization mass spectrometry (ESI-MS) for this purpose has become increasingly popular (*25*). Attractive features of ESI-MS include its high sensitivity and the capability of detecting differentially labeled coexisting protein populations.

ESI in the positive ion mode generates intact, multiply protonated protein ions in the gas phase. This protonation occurs in a structurally sensitive manner; i.e., unfolded solution phase conformations lead to the formation of higher charge states than tightly folded structures (*25*−*28*). Protein ESI charge state distributions recorded under mildly denaturing conditions often exhibit multimodal peak distributions, indicating the presence of coexisting conformations in solution (*29*, *30*).

In many cases, ESI allows the transfer of intact noncovalent complexes into the gas phase, thus making them amenable to direct mass spectrometric analysis (*31*−*35*). Therefore, ESI-MS has the unique capability of monitoring structural changes of a protein in solution, while at the same time providing information on noncovalent interactions with metal ions, prosthetic groups, or other proteins (*36*−*38*). An additional structural dimension is obtained when ESI-MS is used in conjunction with online HDX in continuous labeling experiments (*39*−*42*). The isotope exchange observed in these studies is due to HDX of amide groups, labile side chain hydrogens, and the polypeptide termini.

Online labeling is usually initiated by manual mixing of the protiated protein with a D_2O-based solvent. The time resolution of this manual approach is necessarily limited; typically it is on the order of minutes. To date, it has only been possible to use this technique for monitoring very slow exchange processes, usually employing slightly acidic pH such that k_{ch} is on the order of 0.001 to 1 s^{-1} (*23*, *43*). Structural opening/closing events typically occur on much faster time scales, thus leading to conditions where all of the peaks in the ESI mass spectrum show the same EX2 kinetics (*40*, *42*). A more detailed view of the structural fluctuations occurring under equilibrium conditions is provided in cases where the protein shows a combination of EX1 and EX2 exchange and where distinct HDX kinetics can be observed for coexisting subpopulations. So far, such a behavior has been seen only for proteins exhibiting very slow conformational dynamics (*40*, *44*−*47*).

In this work, ESI-MS is used for continuous labeling experiments on the millisecond time scale. The increased time resolution is achieved through (i) initiation of HDX by rapid online mixing and (ii) labeling of the protein at basic pH where the chemical exchange step is fast, thus favoring EX1 exchange. ESI-MS with rapid online mixing ("time-resolved ESI-MS") has previously been used for studying the unfolding and folding of proteins in kinetic experiments (*48*−*50*). Lin and Dass (*51*) were the first to explore the use of this approach for online HDX experiments, albeit with a moderate time resolution on the order of seconds.

As a model system for this study we chose myoglobin (Mb). The native state of this 153-residue protein is comprised of eight α-helices (A−H) which adopt a largely spherical tertiary structure, forming a hydrophobic pocket into which the heme prosthetic group is noncovalently bound (*52*). Native holomyoglobin (hMb) contains 263 exchangeable hydrogens, 148 of which are located along the amide backbone, 110 on the amino acid side chains, 3 on the termini, and 2 on the heme propionates. The folding and conformational dynamics of both hMb and apomyoglobin (aMb) have been extensively studied (*1*, *10*, *53*−*63*). In the current work, the formation of partially folded Mb conformations is promoted through the presence of an organic cosolvent at slightly basic pH. The interconversion of different conformational and heme binding states is studied by time-resolved ESI-MS with online HDX under equilibrium conditions. We propose a detailed model to quantitatively account for the observed EX1 and EX2 kinetics.

EXPERIMENTAL PROCEDURES

Materials. Ammonium-d_4 deuteroxide, acetic acid-*O*-*d* (Isotec, Inc., Miamisburg, OH), deuterium oxide (Cambridge Isotope Laboratories, Inc., Andover, MA), acetic acid, ammonium hydroxide (Fisher Scientific, Nepean, Ontario, Canada), acetonitrile (Caledon Laboratories, Georgetown, Ontario, Canada), and ammonium acetate (Fluka, Buchs, Switzerland) were used without further purification. Ferrimyoglobin from horse skeletal muscle (Sigma, St. Louis, MO) was dialyzed against 20 mM ammonium acetate and, subsequently, acidified to pH 3.0 with acetic acid prior to the addition of ammonium hydroxide and acetonitrile. The addition of acetic acid was found to significantly enhance signal intensity and decrease peak tailing in the mass spectrum. pH and pD values were measured with an AB15 pH meter (Fisher Scientific, Nepean, Ontario, Canada). Reported values were corrected for isotope effects by using the relation pD = pH meter reading + 0.40 (*64*).

Time-resolved ESI-MS with online HDX was carried out using the continuous flow mixing setup shown in Figure 1. This apparatus is a variation of that used in previous work (*48*, *50*). Briefly, two syringes are advanced simultaneously using syringe pumps (Harvard Apparatus, South Natick, MA). The contents of each syringe are combined at a mixing tee which empties into a fused-silica "labeling capillary" (Polymicro Technologies, Phoenix, AZ) that is connected to the ESI source of the mass spectrometer. Effective mixing at the tee has been demonstrated in previous studies

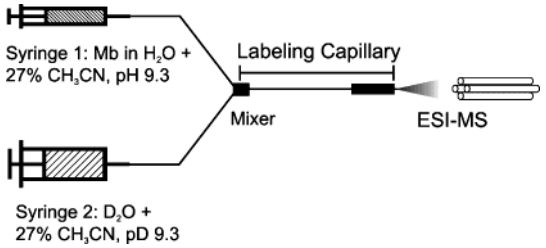

FIGURE 1: Schematic diagram of the continuous flow setup used for time-resolved ESI-MS with online HDX. For details see text.

(*49*, *65*). The duration of the labeling time was controlled by altering the length and the i.d. of the labeling capillary. For labeling times less than 450 ms, a 75 μm i.d. capillary was used. Longer times were achieved with a 100 μm i.d. labeling capillary and a step-down connection to a 75 μm i.d. capillary for the terminal 1.8 cm at the ESI source. During labeling experiments, syringe 1 contained myoglobin in 27% acetonitrile, adjusted to pH 9.3 with NH_4OH, and syringe 2 contained a labeling solution of D_2O with 27% acetonitrile, adjusted to pD 9.3 with ND_4OD. Syringes 1 and 2 were advanced at flow rates of 15 and 290 μL min^{-1}, respectively. These flow conditions resulted in a D_2O content of 95% in the labeling capillary and a total flow rate of 305 μL min^{-1} at the ESI source. Efficient mixing has been demonstrated previously by comparing time-resolved ESI-MS data with results from optical stopped-flow spectroscopy (*49*, *65*, *66*). The distortion of the measured kinetics due to laminar flow effects is small under the conditions of this work (*67*) and was therefore not considered for the data analysis.

The API 365 triple quadrupole mass spectrometer (SCIEX, Concord, Ontario, Canada) used in this study was operated in the positive ion mode. For HDX experiments, individual peaks were measured by scanning selected windows corresponding to 15−50 *m*/*z* units, using a dwell time of 1 ms and step size of 0.2 *m*/*z* units. Typically, 35 scans were averaged for each peak. This source uses pneumatically assisted ESI (with dry air as a nebulizer gas) and an orthogonal flow of air ("turbo gas"), at 10 L min^{-1} at room temperature, to aid desolvation and to reduce the presence of water vapor in the source region. Low declustering voltages were used in the ion sampling interface of the mass spectrometer (orifice-skimmer potential difference 20 V, focusing ring-skimmer potential difference 200 V) to minimize the disruption of noncovalent interactions by collision-induced dissociation (*68*, *69*). A decrease of these voltages by a factor of 2 did not result in significant changes of the observed protein charge state distributions. However, the signal-to-noise ratio of the data recorded under those conditions was significantly lower. A Gaussian fitting procedure was used to determine the maxima of protein peaks after labeling (*50*).

Analytical Ultracentrifugation. Protein samples were prepared as for ESI-MS experiments. Data were collected in an Optima XL-A analytical ultracentrifuge (Beckman, Fullerton, CA). A four-hole An-60Ti rotor and six-channel cells with Epon charcoal centerpieces were used for sedimentation equilibrium experiments. Absorbance measurements were taken in 0.002 cm radial steps. For sedimentation equilibrium experiments, samples were allowed to equilibrate for 18 h at 30000 rpm before data collection. Scans were taken at 30000, 24000, and 16000 rpm with at least 8 h equilibration time at each rotor speed prior to scanning. Data were analyzed using software supplied by the manufacturer. The errors reported for the measured molecular masses correspond to the 95% confidence interval.

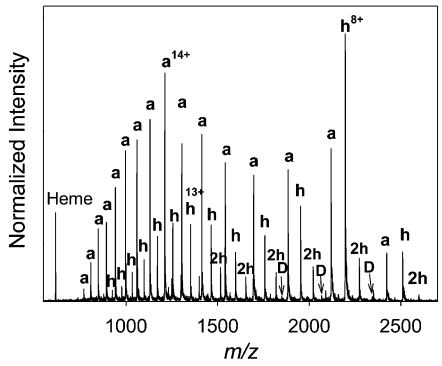

FIGURE 2: Electrospray mass spectrum of partially denatured myoglobin (27% acetonitrile, pH 9.3). Peaks are labeled for clarity. Notation: a, apomyoglobin (aMb); h, holomyoglobin (hMb); 2h, myoglobin carrying two heme groups (2hMb); D, hMb dimer. In the text, highly charged hMb ions (with a maximum at hMb^{13+}) are assigned to the solution phase species hMb_U.

Sedimentation velocity profiles were measured at 60000 rpm at 20 °C in double sector cells. Scans were taken every 10 min for a total analysis time of 190 min. Sedimentation coefficients were calculated from the data obtained using the SVEDBERG software package (*70*) and subsequently converted to $s_{20,w}$ values by standard methods (*71*, *72*). The experimental error of the measured sedimentation coefficients, as determined by the fitting program, was on the order of 1%. Values for solvent viscosity and density were determined using an Ostwald viscometer and pycnometer, respectively [$\eta_{water,20°C} = 1.002$ mPa s, $\rho_{water,20°C} = 0.99821$ g mL^{-1} (*73*); $\eta_{27\%acetonitrile,20°C} = 1.135$ mPa s, $\rho_{27\%\ acetonitrile,20°C} = 0.95889$ g mL^{-1}]. A partial specific volume value of 0.741 mL g^{-1} as calculated in ref *74* was used for all solvents.

RESULTS AND DISCUSSION

Electrospray Mass Spectrometry. The ESI mass spectrum of Mb recorded under mildly denaturing equilibrium conditions [in acetonitrile/water (27:73 v/v) at pH 9.3] shows a wide array of protein ions in charge states ranging from 7+ to 23+ (Figure 2). The complexity of the spectrum is further increased by the observation of several heme binding states. Ions of hMb exhibit a bimodal charge state distribution. The low charge states, around hMb^{8+}, predominantly represent solution phase holoproteins in a native (or nativelike) conformation (*36*, *41*, *49*, *50*, *75*). hMb ions in higher charge states, centered at hMb^{13+}, correspond to proteins that have a more unfolded solution phase structure but still retain their heme group (*49, 65*). This species will be referred to as hMb_U. A bimodal distribution is also observed for aMb ions. Charge states around aMb^{8+} represent a compact state of the apoprotein, whereas peaks centered around aMb^{14+} correspond to more unfolded conformations. Lower intensities are seen for Mb ions with two heme groups attached (termed 2hMb) in charge states ranging from 7+ to 14+. Previous work indicates that this species corresponds to solution phase proteins that are bound to noncovalent heme dimers (*50*). Free heme is observed as a singly charged ion at *m*/*z* 616.2. Close inspection of Figure 2 also reveals the presence of ions corresponding to hMb dimers.

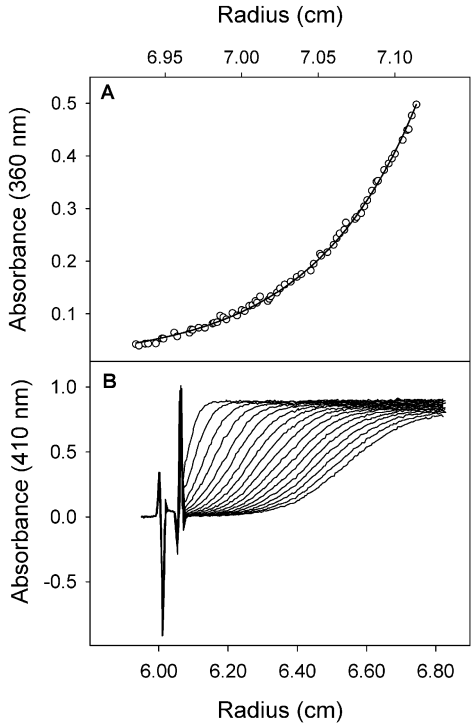

FIGURE 3: (A) Sedimentation equilibrium profile for partially denatured myoglobin (27% acetonitrile, pH 9.3) obtained by analytical ultracentrifugation at 30000 rpm. The solid line represents a single-exponential fit to the experimental data, corresponding to a protein mass of 17.4 ± 0.8 kDa. (B) Sedimentation velocity profiles recorded at 60000 rpm under the same solvent conditions as in (A). Scans were taken every 10 min.

Analytical Ultracentrifugation. Partially folded Mb is known to form noncovalent dimers and larger aggregates under a number of mildly denaturing solvent conditions (*1*, *76*−*78*). Estimating the solution phase abundance of a noncovalent complex based on ESI-MS data is a difficult task (*79*, *80*). Thus, the low abundance of hMb dimer ions in Figure 2 (∼2%) is not sufficient for ruling out extensive protein aggregation in solution. Analytical ultracentrifugation was used for assessing the degree of protein aggregation. Monitoring the absorption in the heme Soret region at 360 nm, we measured sedimentation equilibrium profiles of Mb under the mildly denaturing conditions used for ESI-MS (27% acetonitrile, pH 9.3) at several rotor speeds. Control experiments were carried out on native hMb in aqueous solution containing 100 mM NaCl. Global analysis of results obtained at rotor speeds of 30000, 24000, and 16000 rpm revealed that the equilibrium sedimentation profiles recorded under mildly denaturing and native solvent conditions were well described by single exponentials, corresponding to molecular masses of 17400 ± 800 and 17700 ± 900 Da, respectively (Figure 3A). Virtually the same results were obtained at a detection wavelength of 280 nm, which is dominated by the absorption of aromatic side chains (data not shown). The molecular masses of aMb (16952 Da) and hMb (17568 Da) are within the margin of error for both samples. These data clearly show that Mb under the conditions of the current work predominantly exists as a monomeric species.

Sedimentation velocity profiles obtained for mildly denatured Mb at a detection wavelength of 410 nm are depicted in Figure 3B. These data are very similar to those observed for native control samples (prepared as indicated above; data not shown). Sedimentation coefficients ($s_{20,w}$) obtained from these profiles were 1.84 ± 0.02 and 1.88 ± 0.02 S for partially denatured Mb and for native hMb, respectively. For comparison, a sedimentation coefficient of 0.46 S has been measured for unfolded Mb in 6 M urea at pH 3.0 (*81*). These data, together with the results of recent optical experiments (*82*), indicate that the overall compactness and shape of Mb under the mildly denaturing conditions used here are similar to that of the native protein. At first sight, this conclusion seems surprising given the appearance of the ESI mass spectrum in Figure 2, which clearly indicates the presence of non-native protein subpopulations. However, the degree of unfolding appears to be moderate, since the maximum of the aMb charge state distribution is only located at 14+. Higher charge states (around 19+) have been reported for more extensively unfolded Mb (*36*, *41*, *65*). Also, the ESI mass spectrum in Figure 2 likely overemphasizes the presence of non-native proteins, partly because unfolded conformations are expected to result in higher ion intensities (*83*) but also because the sensitivity of quadrupole mass analyzers is thought to drop with increasing *m*/*z* (*84*).

Another interesting result is that analytical ultracentrifugation does not indicate the presence of free heme, which would be manifested as an elevated baseline. This is compatible with the results of recent diffusion studies that also indicate that heme and protein remain associated under the mildly denaturing conditions used here (*82*). In contrast, a fairly strong signal for free heme is observed in the ESI mass spectrum (Figure 2). A possible explanation for this observation is that some of the aMb ions observed by ESI-MS may represent very loosely associated heme−protein complexes in solution that underwent separation during ESI. For reasons of simplicity we will continue to use the term "apomyoglobin" (aMb), thereby explicitly including solution phase proteins that may have very weak residual heme−protein interactions.

Hydrogen−Deuterium Exchange Kinetics. The mass spectrum (Figure 2) does not provide any information on the conformational dynamics of Mb. Time-resolved ESI-MS was therefore employed to monitor the HDX kinetics of Mb in acetonitrile/D_2O (27:73 v/v) at pD 9.3. The average chemical exchange rate k_{ch} for unprotected amide hydrogens in Mb at this pD, and for a temperature of 25° C, is 644 s^{-1}, as calculated on the basis of the data provided by Bai et al. (*23*). Labile side chain hydrogens are expected to exchange with rates that are similar or even faster (*85*). Observation times ranging from 7 ms to 3.1 s after initiation of labeling were studied by time-resolved ESI-MS. In addition, measurements corresponding to $t = 1.5$ h were taken in manual mixing experiments.

The exchange behavior observed for different ions in the spectrum can be grouped into two categories (Figure 4). (i) With increasing labeling time, the peak maxima of aMb, 2hMb, and hMb_U shift to higher mass, indicating EX2 exchange, i.e., the occurrence of rapid unfolding/refolding events with closing rate constants $k_{cl} \gg 644$ s^{-1}. As an example, data obtained for aMb^{14+} are depicted in Figure 4A−D. (ii) A more complex exchange behavior is seen for hMb ions in charge states 7+ to 9+, as exemplified by hMb^{8+} in Figure 4E−H. For labeling times up to 3.1 s, these protein ions show bimodal mass distributions. The gradual shift of both peaks to higher mass again indicates the occurrence of rapid structural fluctuations (EX2 exchange).

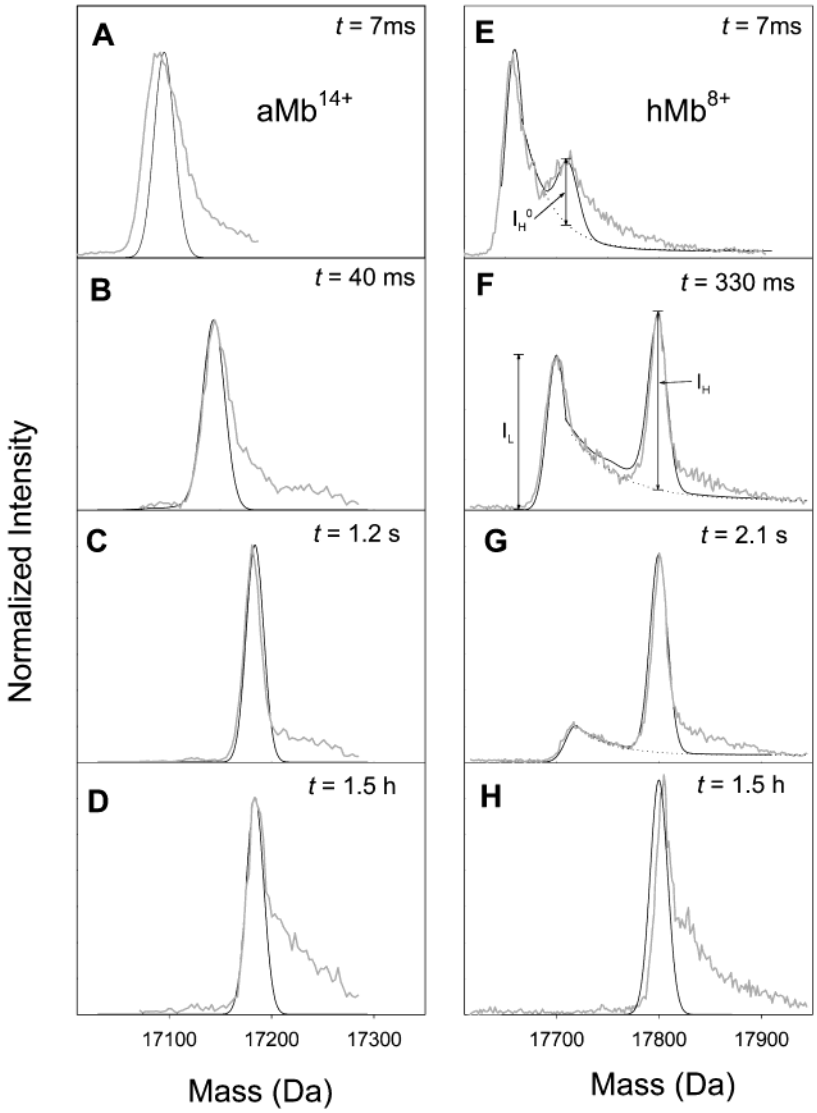

FIGURE 4: Isotope exchange behavior observed for the ions aMb^{14+} (A−D) and hMb^{8+} (E−H) for selected time points. Noisy lines in dark gray represent experimental data. Smooth black lines are simulated peak shapes, calculated from a kinetic model (Figure 6). Intensities of hMb^{8+} low and high mass peaks are denoted as I_L and I_H, respectively. Determination of I_H in panels E−H: Peak tailing of the low mass peaks due to the presence of incompletely desolvated ions contributes to the intensities of the high mass peaks. To obtain suitable baselines for the determination of I_H, the tailing ends of the low mass peaks were extrapolated by using fitted expressions of the form $y = c + \exp(-a \times \text{mass})$, as indicated by the dotted lines. These extrapolations were used for the determination of I_H, as exemplified in panel E. The intensity of the high mass peak for $t = 7$ ms, as determined by this method, is denoted as I_H^0. The fitted baselines were included in the simulated curves shown in panels E−H.

In addition, the relative intensity of the low mass peak decreases, and that of the high mass peak increases (EX1 behavior; see ref *86*). The latter observation shows that the corresponding solution phase proteins are also involved in slow unfolding/refolding processes with $k_{cl} \ll 644\ s^{-1}$. The low mass peak is no longer detectable for $t = 1.5$ h.

Figure 5A provides a synopsis of the observed EX2 exchange processes. The HDX kinetics measured for all aMb, 2hMb, and hMb_U ions, as well as for the *high mass* peaks of hMb^{7+} to hMb^{9+}, are virtually identical. The upper curve in Figure 5A shows plots of representative peak maxima as a function of labeling time. These data are well described by the single-exponential fit

$$\text{mass shift} = 125 + 108[1 - \exp(-23.3t)] \qquad (4)$$

which is shown as a solid line in Figure 5A (upper curve). All of these ions show a maximum of ca. 233 exchanged hydrogens after a labeling time of less than 1 s. Taking into account the 95% deuterium content of the labeling solvent and the total number (263) of exchangeable sites in Mb, this corresponds to a relative exchange level of $233/(263 \times 0.95) = 93\%$. This exchange level is very close to the values that were observed when the observation time was extended to 1.5 h. For the conditions of this work, some back-exchange with residual water vapor in the ESI source is unavoidable (*39*, *50*). Therefore, an exchange level around 93% represents virtually complete labeling of the protein. According to eq 4, 108 labile sites undergo EX2 exchange with a rate constant of $k_{ex} = 23.3\ s^{-1}$.[2] Burst phase labeling occurs for 125

[2] Here and in the remainder of the text, numbers of hydrogens correspond to measured values. For comparison with the actual number of sites in the protein, the quoted figures should be multiplied by a factor of $263/233 = 1.13$, where 263 is the total number of exchangeable sites in Mb and 233 is the maximum number of exchange events observed.

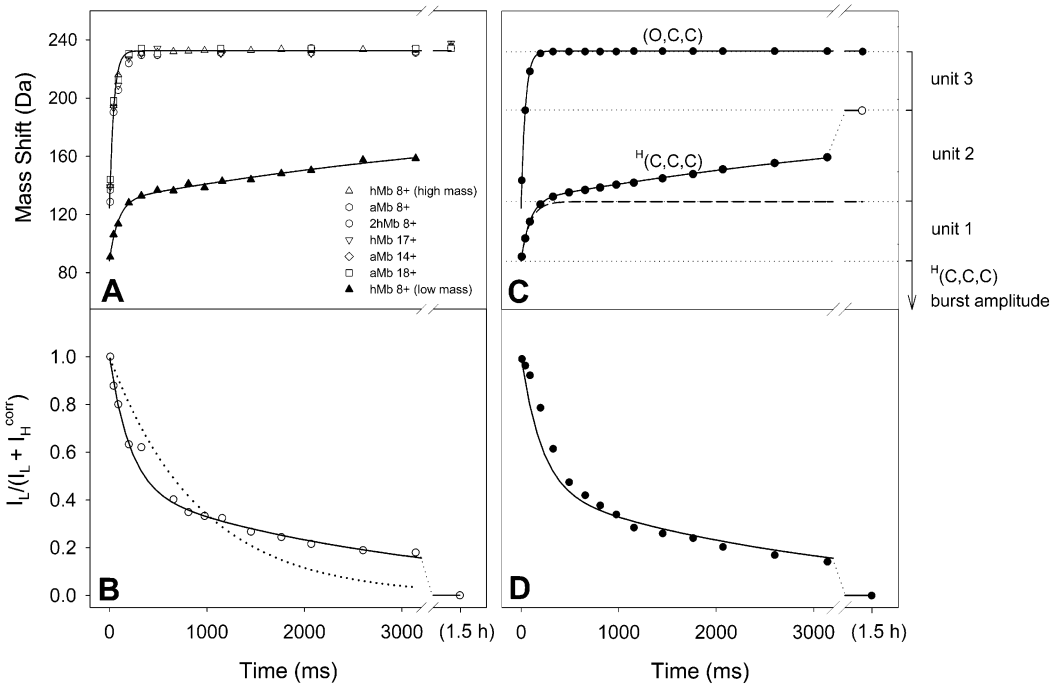

FIGURE 5: Panels A and B illustrate the HDX kinetics measured for partially denatured myogobin. (A) EX2 kinetics observed for various ions. Solid lines are fits corresponding to eq 4 (upper curve) and eq 5 (lower curve). (B) EX1 kinetics observed for hMb^{8+}. Notation: I_L, intensity of low mass peak; I_H^{corr}, corrected intensity of high mass peak. The solid line is a biexponential fit to the experimental data, corresponding to eq 6. A single-exponential fit (dotted line) is inadequate for describing the observed kinetics. Panels C and D show the results of HDX simulations based on a kinetic model (Figure 6). Solid lines represent fits to the experimental data (taken from panels A and B); solid circles are simulation results. (C) Upper curve, EX2 kinetics for (O,C,C); lower curve, EX2 kinetics for ^{H}(C,C,C). Unit 1 represents the hydrogens labeled during the fast phase of the ^{H}(C,C,C) EX2 exchange (dashed curve). Unit 2 corresponds to sites that undergo exchange during the slow phase (see eq 5). The remaining sites represent unit 3. (D) EX1 kinetics of ^{H}(C,C,C).

hydrogens. The observation of identical exchange kinetics for the different charge and heme binding states suggests that the corresponding solution phase species (aMb, 2hMb, and hMb_U) interconvert on a time scale much shorter than $k_{ex}^{-1} \approx 40$ ms (*40*). The case of the *high mass* peaks of hMb^{7+} to hMb^{9+} (which show the same HDX behavior) will be discussed below.

The lower curve in Figure 5A exemplifies the EX2 kinetics observed for the *low mass* peaks of hMb^{8+}. The fit to these data is given by the biexponential expression

$$\text{mass shift} = 88 + 41[1 - \exp(-11.1t)] + 63[1 - \exp(-0.2t)] \quad (5)$$

Very similar kinetics were observed for hMb^{7+} and hMb^{9+} (data not shown). Burst phase labeling occurs for only 88 sites, which is significantly less than the burst phase amplitude of 125 sites seen for all other protein ions. This observation confirms that the low mass peaks of hMb^{7+} to hMb^{9+} represent solution phase proteins that have a more nativelike conformation than the other species observed. A group of 41 hydrogens exchanges with a rate constant of $k_{ex} = 11.1\ s^{-1}$, while a second group comprising 63 sites undergoes slower exchange with $k_{ex} = 0.2\ s^{-1}$. It is noted that the value of the second rate constant in eq 5 cannot be determined accurately, because the disappearance of the low mass peaks limits the experimental time window to ~3 s. Acceptable fits were obtained for k_{ex} values ranging from 0.1 to 0.3 s^{-1}. The value of 0.2 s^{-1} in eq 5 represents the midpoint of this range.

A number of factors have to be taken into account for the analysis of the EX1 kinetics observed for the hMb^{7+} to hMb^{9+} ions. The determination of the high and low mass relative peak intensities (I_H and I_L, respectively) requires the use of a baseline correction, which is outlined in the caption of Figure 5. In addition, the high mass peaks observed for very early labeling times (e.g., for $t = 7$ ms; Figure 4E) clearly represent the "tail end" of the hMb_U charge state distribution. As the labeling time is increased, however, the high mass peaks contain an increasing contribution from nativelike proteins that have spent time in a more unfolded conformation during labeling but have attained a nativelike structure immediately prior to ionization. Only this second contribution is of interest for analyzing the EX1 kinetics. Therefore, corrected relative intensities for the high mass peaks, I_H^{corr}, were determined according to $I_H^{corr} = I_H - I_H^0$. The $t = 7$ ms time point was used to estimate an I_H^0 value corresponding to 24% of the total hMb^{8+} peak intensity.

Figure 5B shows a plot of $I_L/(I_L + I_H^{corr})$. Surprisingly, a monoexponential fit did not adequately describe these data, and a biphasic expression had to be used instead. The solid line shown in Figure 5B corresponds to the equation

$$I_L/(I_L + I_H^{corr}) = 0.55[1 - \exp(-3.6t)] + 0.43[1 - \exp(-0.31t)] \quad (6)$$

The simplest explanation for this behavior is the assumption of two different subpopulations of proteins, one undergoing a cooperative opening event with $k_{op} = 3.6\ s^{-1}$ and the other with $k_{op} = 0.31\ s^{-1}$. Although the reasons underlying this kinetic heterogeneity are not clear, it is interesting to note

that hMb under the conditions of our work likely represents a mixture of proteins with their heme groups in a non-native orientation (rotated by 180° about the heme α−γ-meso axis) and in the correct binding geometry (*87*−*89*). The two heme binding states are almost isoenergetic and interconvert on a time scale of hours. It seems possible that the two forms of the protein show different EX1 opening rates, especially since the opening event is thought to involve the heme binding region of the protein (see below). However, without further experimental evidence this explanation remains speculative.

Kinetic Modeling. According to thermodynamic principles, the native conformation of any protein must be in dynamic equilibrium with higher energy conformations that represent different degrees of unfolding (*16*, *20*). Recent NMR-based native state HDX studies indicate that protein structures can be dissected into a number of distinct (un)folding units. The stepwise sequential opening of all units in the order of their thermodynamic stability leads from the native conformation to the unfolded state; the reverse process leads to protein refolding under equilibrium conditions (*16*, *20*, *90*−*93*). Transient opening events of individual units briefly expose well-defined groups of exchangeable hydrogens to the solvent, thus allowing HDX to occur as expressed in eq 1. This general model of equilibrium structural dynamics is also expected to apply under mildly denaturing conditions that promote the population of partially unfolded protein molecules.

Unfolding Units in Myoglobin. Previous studies have identified a minimum of four distinct Mb conformations, which may be arranged in the sequence shown in Scheme 1 according to their degree of unfolding (*1*, *10*, *53*, *94*, *95*).

Scheme 1

$$\mathrm{hMb_N} \underset{+\mathrm{heme}}{\overset{-\mathrm{heme}}{\rightleftharpoons}} \mathrm{aMb_N} \rightleftarrows \mathrm{aMb_I} \rightleftarrows \mathrm{aMb_U}$$

In this scheme $\mathrm{hMb_N}$ represents the native, tightly folded heme−protein complex. In the absence of heme, and under physiological solvent conditions, the protein adopts the state $\mathrm{aMb_N}$, which has an overall structure resembling the compact native fold but has extensively disordered elements in the heme binding region. Helix F, in particular, fluctuates between nativelike and more disordered conformations (*10*). The molten globule $\mathrm{aMb_I}$ becomes most strongly populated around pH 4.0; this state represents the next level of unfolding (*1*). Structured regions in $\mathrm{aMb_I}$ include the A, G, and H helices. Finally, the fully unfolded protein is represented by $\mathrm{aMb_U}$ (*62*). The sequence $\mathrm{aMb_N} \leftarrow \mathrm{aMb_I} \leftarrow \mathrm{aMb_U}$ provides a minimalist description of the kinetic aMb folding mechanism in heme-free solution (*53*). It has been shown that the three structural transitions in Scheme 1 are associated with the exposure of three distinct populations of hydrogens (*54*). We therefore suggest a model where the Mb structure is dissected into three unfolding units. Each unit can be in an open (O) or in a closed (C) conformation. Unit 1 encompasses the heme binding region (*10*), unit 3 includes the A−G−H folding core (*1*), and the remaining structural elements of the protein are assigned to unit 2. Within this framework, the conformational transitions of Scheme 1 may therefore be expressed as shown in Scheme 2.

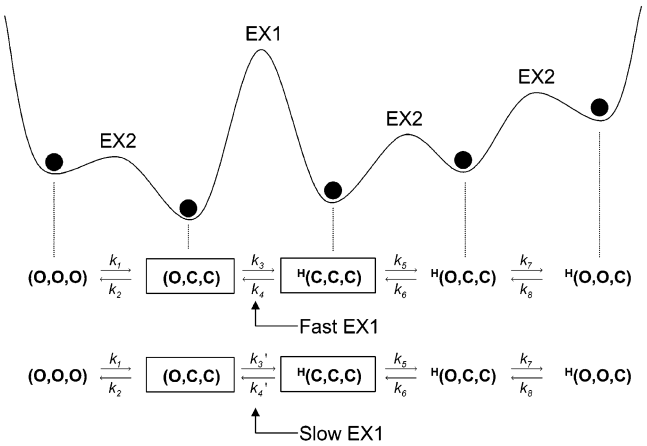

FIGURE 6: Schematic free energy profile of Mb conformations and kinetic model of the conformational dynamics under mildly denaturing conditions (27% acetonitrile, pH 9.3). The model assumes two independent parallel reaction sequences that do not interact on the experimental time scale of roughly 3 s. The vector notation used for the various protein states indicates which of the three (un)folding units are in open (O) and closed (C) conformations. The presence of a heme group is indicated by a superscript H. Only those species marked in boxes are significantly populated such that they can be observed in the ESI mass spectrum (see Table 1). Most of the peak intensity of hMb ions in charge states 7+ to 9+ is attributed to the solution phase conformation ^{H}(C,C,C); aMb ions are assigned to (O,C,C). The values of the rate constants k_i are summarized in Table 1.

Scheme 2

$$^{\mathrm{H}}(\mathrm{C,C,C}) \underset{+\mathrm{heme}}{\overset{-\mathrm{heme}}{\rightleftharpoons}} (\mathrm{O,C,C}) \rightleftarrows (\mathrm{O,O,C}) \rightleftarrows (\mathrm{O,O,O})$$

In this scheme the superscript H indicates the presence of the heme group. It is noted that most previous studies were exclusively focused on amide HDX, whereas the technique employed here is sensitive to exchange of *all* labile hydrogens, including those located in side chains. For this reason, the total number of exchangeable sites assigned to each of the three units cannot be directly compared to literature data (e.g., ref *54*).

The assumption of three distinct (un)folding units in Mb, undergoing transient opening/closing events, implies a kinetic model for the structural dynamics of the protein under the conditions of the current study (Figure 6). In the following sections, it will be outlined how the HDX kinetics of the two major species, hMb and aMb, can be interpreted within this model. The remaining two species, 2hMb and $\mathrm{hMb_U}$, will also be addressed. We will present the results of detailed computer simulations, which confirm that the predictions made by the model are in excellent agreement with the experimentally observed exchange kinetics.

HDX Kinetics of hMb. Proteins corresponding to the low mass peaks of $\mathrm{hMb^{7+}}$ to $\mathrm{hMb^{9+}}$ are assigned to the solution phase structure ^{H}(C,C,C). We propose that the EX1 kinetics observed for this species are mediated by slow opening events affecting unit 1, i.e., the heme binding region of the protein. This opening event and the concurrent loss of the heme group lead to the structure (O,C,C). Following the discussion above, the biphasic nature of this opening process implies the presence of two different forms of ^{H}(C,C,C). Accordingly, the kinetic model (Figure 6) has two parallel reaction sequences that are kinetically separated on the experimental time scale of roughly 3 s. According to eq 6,

the number ratio of proteins participating in the first sequence (fast EX1 exchange, $k_{op} = 3.6\ s^{-1}$) and the second sequence (slow EX1 exchange, $k_{op} = 0.31\ s^{-1}$) is 0.55:0.43. The two sequences are assumed to be kinetically equivalent, except for the transitions between (O,C,C) and ^{H}(C,C,C).

The biphasic EX2 exchange of ^{H}(C,C,C) is attributed to sequential sub-millisecond fluctuations involving units 1 and 2. It appears likely that the heme group remains in close spatial contact with the protein during the very brief time periods that these units adopt open conformations. We therefore use the notation ^{H}(O,C,C) and ^{H}(O,O,C) for these two species to denote the presence of the heme. According to eq 5, unfolding of unit 1 involves a total of 41 sites that exchange with $k_{ex} = 11.1\ s^{-1}$. Unit 2 involves 63 sites that exchange with $k_{ex} = 0.2\ s^{-1}$. An additional 88 sites are permanently unprotected and undergo burst phase labeling. Presumably, this group includes many of the labile hydrogens located in amino acid side chains, but it may also include some amide hydrogens. The remaining sites (i.e., 233 − 41 − 63 − 88 = 41) are assigned to unit 3. The opening of unit 3 is a rare event that does not significantly contribute to isotope exchange of ^{H}(C,C,C) on the experimental time scale of ca. 3 s.

HDX Kinetics of aMb. We suggest that the bimodal charge state distribution of aMb ions in Figure 2 represents a state comparable to aMb_N in Scheme 1, having the folding pattern (O,C,C). This assignment is compatible with published ESI charge state distributions of aMb under native solvent conditions (*29*, *41*, *96*). The number of sites undergoing burst phase labeling for this species is expected to be 41 + 88 = 129, corresponding to the hydrogens in unit 1 plus those of the burst sites in ^{H}(C,C,C). This prediction is in good agreement with the measured burst phase amplitude of 125 sites. Within our model, the single-exponential EX2 kinetics of (O,C,C) are mediated by rapid unfolding/refolding transitions simultaneously affecting units 2 and 3. The total number of 63 + 41 = 104 sites in these two units is close to the experimentally determined value of 108 hydrogens participating in this exchange process (eq 4). It is well known that a destabilization of the protein structure can suppress subglobal opening/closing events, instead favoring more global conformational transitions (*15*, *16*, *97*). Therefore, the occurrence of structural fluctuations simultaneously involving units 2 and 3 for (O,C,C) is not surprising, keeping in mind that the removal of the heme group significantly reduces the stability of Mb (*55*).

Computer Implementation of the Model. A simulation program was developed to test the numerical predictions of the model described. Within this program, proteins are represented as bit strings. Each bit corresponds to an exchangeable site that is occupied either by hydrogen (0) or by deuterium (1). The strings are divided into three regions, containing 41, 63, and 41 bits, corresponding to units 1, 2, and 3, respectively (Figure 7). In addition, each bit string carries information that determines the opening state of the three units for each protein and whether it belongs to the ensemble undergoing fast or slow EX1 exchange. A simulation was carried out on 2000 bit strings by using the kinetic parameters summarized in Table 1. The number of proteins assigned to each kinetic species was determined in accordance with the corresponding K_{op} values. For the three EX2 transitions, K_{op} was determined from eq 2 on the basis of the measured values of k_{ex} and by using $k_{ch} = 644\ s^{-1}$. The k_{cl} values for these three transitions, i.e., k_1, k_6, and k_8, were taken as $10^5\ s^{-1}$ to ensure that the conditions for EX2 exchange were met. Together with the corresponding K_{op} values, this choice of k_{cl} determines the rate constants of the corresponding opening events.

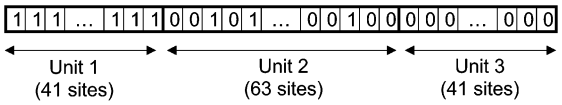

FIGURE 7: Bit string representation of proteins used for the kinetic modeling. 1 and 0 stand for deuterated and protiated sites, respectively. For time $t = 0$, the protein is fully protiated, and all bits have a value of 0. As HDX proceeds, more and more bits are converted from 0 to 1.

Table 1: Parameters Used for Kinetic Simulations[a]

protein state	equilibrium parameters: K_{op}	relative population	$\Delta G°_{app}$ (kJ mol^{-1})[d]	rate constants: k_{cl} (s^{-1})[e]	k_{op} (s^{-1})
(O,O,O)		0.036			
⇃↾	0.036[b]		8.2	$k_1 = 10^5$	$k_2 = 3600$
(O,C,C)		1.0			
⇃↾	3.0[c]		−2.7	$k_3 = 1.2$	$k_4 = 3.6$
				$k_3' = 0.10$	$k_4' = 0.31$
^{H}(C,C,C)		0.33			
⇃↾	0.017[b]		10.1	$k_6 = 10^5$	$k_5 = 1700$
^{H}(O,C,C)		0.006			
⇃↾	0.018[b]		9.9	$k_8 = 10^5$	$k_7 = 1800$
^{H}(O,O,C)		10^{-4}			

[a] Refer to Figure 6 for more information on the model employed. [b] Calculated on the basis of eq 2 from the measured EX2 rate constants by assuming that $k_{ch} = 644\ s^{-1}$ (*23*). [c] Determined as described in the text. [d] Calculated from $\Delta G°_{app} = -RT \ln(K_{op})$. [e] The values of k_1, k_6, and k_8 were taken as $10^5\ s^{-1}$ to ensure that the conditions for EX2 exchange ($k_{cl} \gg k_{ch}$) were met.

The rate constants k_{op} for the EX1 transitions (k_4 and k_4') can be taken from eq 6. The determination of the corresponding k_{cl} values requires knowledge of the concentration ratio of ^{H}(C,C,C) to (O,C,C). On the basis of the ESI mass spectrum, the intensity ratio of these two species is 0.23, implying that $K_{op} = 4.3$. However, this number probably does not adequately reflect the concentration ratio of the two species in solution, as ESI-MS likely overemphasizes the contribution of aMb_N (*29*, *83*). We therefore arbitrarily used a somewhat lower value of $K_{op} = 3.0$. For the kinetic simulations this parameter is almost insignificant, because the EX1 kinetics are only determined by the opening rate constants (k_4 and k_4'). With this choice of K_{op}, (O,C,C) has an apparent $\Delta G°$ that is 2.7 kJ/mol lower than that of the native state ^{H}(C,C,C). It is important to point out that, except for the EX1 equilibrium constant, all of the numerical input values used for our simulation are directly based on experimentally determined parameters. In other words, *the predictions of the kinetic model do not depend on any adjustable factors*.

The simulation was run in iteration steps corresponding to $\Delta\tau = 50$ ns. During each of these steps, individual unlabeled sites can undergo exchange with a probability, W, which is zero if the corresponding unit is in a closed conformation. For sites located in an open unit, W is given by

$$W = 1 - \exp(-k_{ch}\Delta\tau) \qquad (7)$$

The conformational dynamics of the protein were modeled during each iteration by giving every protein the chance to convert to an adjacent species. The probability for each of these transitions is determined by the corresponding rate constant k_i in a manner analogous to eq 7. For reasons of simplicity, all subglobal conformational transitions were assumed to be cooperative events (*20*). Simulated mass distributions of ^{H}(C,C,C) and (O,C,C) were calculated for selected time points by counting the number of exchanged sites in each protein (i.e., the number of bits having a value of 1). The presence of sites permanently adopting an exchange-competent state was taken into account by adding 88 Da to the calculated mass values (see eq 5). The contribution of each protein to the overall simulated mass distributions was taken as a Gaussian peak with an fwhm of 20 Da.

Simulated mass distributions for selected time points are depicted in Figure 4, together with the corresponding experimental data. The calculated distributions shown in panels A−D represent (O,C,C). Panels E−H show calculated distributions for ^{H}(C,C,C), taking into account the expected contribution from overlapping hMb_U proteins for the high mass peak. The simulated EX2 kinetics for ^{H}(C,C,C) and (O,C,C) are shown in Figure 7A, together with the corresponding fits to the experimental data, taken from Figure 5A. Finally, the simulated EX1 kinetics of ^{H}(C,C,C) are compared to the actual fit of the corresponding measured data in Figure 7B. The excellent overall agreement between experimental and simulated results indicates that the observed dynamics are consistent with the proposed kinetic model (Figure 6). While this agreement does not provide direct proof of the model, it does at least attest to the self-consistency of the general framework used.

Although our simulation does not explicitly take into account the species hMb_U and 2hMb, the extension of the proposed model to include these two forms of the protein is straightforward. The fact that they both show HDX kinetics that are indistinguishable from those of the apoprotein shows that hMb_U, 2hMb, and aMb(O,C,C) are in rapid equilibrium. From our data it cannot be determined if these species should be interpreted as on-pathway or off-pathway with respect to the linear reaction sequences (Figure 6). Both of these cases are kinetically equivalent, as long as the interconversion with (O,C,C) occurs on a time scale that is rapid compared to $k_{ex}^{-1} \approx 40$ ms (*98*).

CONCLUSIONS

To the best of our knowledge, this is the first report of ESI-MS-based online HDX experiments with millisecond time resolution. This approach provides a powerful tool for monitoring protein structural dynamics under mildly denaturing equilibrium conditions. At basic pH, chemical exchange is rapid, thus facilitating the differentiation between conformational fluctuations occurring on different time scales (i.e., EX1 and EX2 processes). The approach employed in this study allows the correlation of three complementary structural probes: the ESI charge state distribution, ligand binding state, and isotope exchange kinetics. All of this information is obtained simultaneously for coexisting protein conformations in solution. Our work does not provide direct information on the spatial hydrogen/deuterium distribution after labeling. However, this type of information should be obtainable by using the described approach in conjunction with online fragmentation of gas phase protein ions (*99*). Experimental efforts in this direction are currently underway in our laboratory. These studies will prove or disprove the tentative assignments of the proposed three unfolding units to specific structural regions within the protein.

The data presented in this study provide a complex picture of the conformational dynamics of Mb under mildly denaturing conditions (27% acetonitrile, pH 9.3). A detailed kinetic model has been developed that is consistent with a wide range of previous studies from the literature. It suggests that the two major species observed in the mass spectrum, assigned to the structures (O,C,C) and ^{H}(C,C,C), are both in rapid (EX2) equilibrium with more unfolded conformations, separated from their respective "ground states" through relatively low free energy barriers. In contrast, the transition between these two states represents a slow (EX1) process that corresponds to a much higher barrier (Figure 6). Recent work suggests that proteins may cross major free energy barriers not by surmounting them but by circumventing them through a long diffusive journey on a multidimensional energy landscape (*100*). Slow conformational transitions could therefore be mediated by rapid, thermally activated structural dynamics. Such a view is consistent with the model suggested in this work, where rapid structural fluctuations on each side of a major barrier may represent conformational sampling processes that on rare occasions result in barrier crossing.

ACKNOWLEDGMENT

The analytical ultracentrifugation experiments presented here were carried out at the UWO Biomolecular Interactions and Conformation Facility.

REFERENCES

1. Hughson, F. M., Wright, P. E., and Baldwin, R. L. (1990) *Science 249*, 1544−1548.
2. Bucciantini, M., Giannoni, E., Chiti, F., Baroni, F., Formigli, L., Zurdo, J., Taddei, N., Ramponi, G., Dobson, C. M., and Stefani, M. (2002) *Nature 416*, 507−511.
3. Hill, T. J., Lafitte, D., Wallace, J. I., Cooper, H. J., Tsvetkov, P. O., and Derrick, P. J. (2000) *Biochemistry 39*, 7284−7290.
4. Wright, P. E., and Dyson, H. J. (1999) *J. Mol. Biol. 293*, 321−331.
5. Dyson, H. J., and Wright, P. E. (1998) *Nat. Struct. Biol. 5*, 499−503.
6. Dyson, H. J., and Wright, P. E. (2002) *Curr. Opin. Struct. Biol. 12*, 54−60.
7. Dunker, A. K., and Obradovic, A. (2001) *Nat. Biotechnol. 19*, 805−806.
8. Brutscher, B., Brüschweiler, R., and Ernst, R. R. (1997) *Biochemistry 36*, 13043.
9. Barbar, E., Hare, M., Daragan, V., Barany, G., and Woodward, C. (1998) *Biochemistry 37*, 7822−7833.
10. Eliezer, D., Yao, J., Dyson, H. J., and Wright, P. E. (1998) *Nat. Struct. Biol. 5*, 148−155.
11. Tollinger, M., Skrynnikov, N. R., Mulder, F. A. A., Forman-Kay, J. D., and Kay, L. E. (2001) *J. Am. Chem. Soc. 123*, 11341−11352.
12. Mayo, S., and Baldwin, R. L. (1993) *Science 262*, 873−876.
13. Li, R., and Woodward, C. (1999) *Protein Sci. 8*, 1571−1590.
14. Englander, S. W., Sosnick, T. R., Englander, J. J., and Mayne, L. (1996) *Curr. Opin. Struct. Biol. 6*, 18−23.
15. Miller, D. W., and Dill, K. A. (1995) *Protein Sci. 4*, 1860−1873.
16. Bai, Y., Sosnick, T. R., Mayne, L., and Englander, S. W. (1995) *Science 269*, 192−197.
17. Parker, M. J., and Marqusee, S. (2001) *J. Mol. Biol. 305*, 593−602.
18. Xu, Y., Mayne, L., and Englander, S. W. (1998) *Nat. Struct. Biol. 5*, 774−778.

19. Engen, J. R., and Smith, D. L. (2001) *Anal. Chem. 73*, 256A−265A.
20. Englander, S. W., Mayne, L., and Rumbley, J. N. (2002) *Biophys. Chem. 101*−*102*, 57−65.
21. Maity, H., Lim, W. K., Rumbley, J. N., and Englander, S. W. (2003) *Protein Sci. 12*, 153−160.
22. Hvidt, A., and Nielsen, S. O. (1966) *Adv. Protein Chem. 21*, 287−386.
23. Bai, Y., Milne, J. S., Mayne, L., and Englander, S. W. (1993) *Proteins: Struct., Funct., Genet. 17*, 75−86.
24. Bieri, O., and Kiefhaber, T. (2001) *J. Mol. Biol. 310*, 919−935.
25. Kaltashov, I. A., and Eyles, S. J. (2002) *Mass Spectrom. Rev. 21*, 37−71.
26. Chowdhury, S. K., Katta, V., and Chait, B. T. (1990) *J. Am. Chem. Soc. 112*, 9012−9013.
27. Konermann, L., and Douglas, D. J. (1997) *Biochemistry 36*, 12296−12302.
28. Grandori, R. (2003) *J. Mass. Spectrom. 38*, 11−15.
29. Dobo, A., and Kaltashov, I. A. (2001) *Anal. Chem. 73*, 4763−4773.
30. Grandori, R. (2002) *Protein Sci. 11*, 453−458.
31. Loo, J. A. (2000) *Int. J. Mass Spectrom. 200*, 175−186.
32. Zhang, Z., Krutchinsky, A., Endicott, S., Realini, C., Rechsteiner, M., and Standing, K. G. (1999) *Biochemistry 38*, 5651−5658.
33. Rostom, A. A., Fucini, P., Benjamin, D. R., Juenemann, R., Nierhaus, K. H., Hartl, F. U., Dobson, C. M., and Robinson, C. V. (2000) *Proc. Natl. Acad. Sci. U.S.A. 97*, 5185−5190.
34. van Berkel, W. J. H., van den Heuvel, R. H. H., Versluis, C., and Heck, A. J. R. (2000) *Protein Sci. 9*, 435−439.
35. Daniel, J. M., Friess, S. D., Rajagopalan, S., Wendt, S., and Zenobi, R. (2002) *Int. J. Mass Spectrom. 216*, 1−27.
36. Feng, R., and Konishi, Y. (1993) *J. Am. Soc. Mass Spectrom. 4*, 638−645.
37. Vis, H., Heinemann, U., Dobson, C. M., and Robinson, C. V. (1998) *J. Am. Chem. Soc. 120*, 6427−6428.
38. Nemirovskiy, O. V., Ramanathan, R., and Gross, M. L. (1997) *J. Am. Soc. Mass Spectrom. 8*, 809−812.
39. Katta, V., and Chait, B. T. (1993) *J. Am. Chem. Soc. 115*, 6317−6321.
40. Wagner, D. S., and Anderegg, R. J. (1994) *Anal. Chem. 66*, 706−711.
41. Wang, F., and Tang, X. (1996) *Biochemistry 35*, 4069−4078.
42. Babu, K. R., and Douglas, D. J. (2000) *Biochemistry 39*, 14702−14710.
43. Smith, D. L., Deng, Y., and Zhang, Z. (1997) *J. Mass Spectrom. 32*, 135−146.
44. Eyles, S. J., Dresch, T., Gierasch, L. M., and Kaltashov, I. A. (1999) *J. Mass Spectrom. 34*, 1289−1295.
45. Eyles, S. J., Speir, J. P., Kruppa, G. H., Gierasch, L. M., and Kaltashov, I. A. (2000) *J. Am. Chem. Soc. 122*, 495−500.
46. Maier, C. S., Schimerlik, M. I., and Deinzer, M. L. (1999) *Biochemistry 38*, 1136−1143.
47. Kim, M.-Y., Maier, C. S., Reed, D. J., and Deinzer, M. L. (2002) *Protein Sci. 11*, 1320−1329.
48. Konermann, L., Collings, B. A., and Douglas, D. J. (1997) *Biochemistry 36*, 5554−5559.
49. Sogbein, O. O., Simmons, D. A., and Konermann, L. (2000) *J. Am. Soc. Mass Spectrom. 11*, 312−319.
50. Simmons, D. A., and Konermann, L. (2002) *Biochemistry 41*, 1906−1914.
51. Lin, H., and Dass, C. (2001) *Rapid Commun. Mass Spectrom. 15*, 2341−2346.
52. Evans, S. V., and Brayer, G. D. (1990) *J. Mol. Biol. 213*, 885−897.
53. Jennings, P. A., and Wright, P. E. (1993) *Science 262*, 892−896.
54. Tsui, V., Garcia, C., Cavagnero, S., Siuzdak, G., Dyson, H. J., and Wright, P. E. (1999) *Protein Sci. 8*, 45−49.
55. Johnson, R. S., and Walsh, K. A. (1994) *Protein Sci. 3*, 2411−2418.
56. Jamin, M., and Baldwin, R. L. (1996) *Nat. Struct. Biol. 3*, 613−618.
57. Feng, Z., Butler, M. C., Alam, S. L., and Loh, S. N. (2001) *J. Mol. Biol. 314*, 153−166.
58. Gilmanshin, R., Gulotta, M., Dyer, R. B., and Callender, R. H. (2001) *Biochemistry 40*, 5127−5136.
59. Nishimura, C., Dyson, H. J., and Wright, P. E. (2002) *J. Mol. Biol. 322*, 483−489.
60. Fishburn, A. L., Keeffe, J. R., Lissonouv, A. V., Peyton, D. H., and Anthony-Cahill, S. J. (2002) *Biochemistry 41*, 13318−13327.
61. Schwarzinger, S., Wright, P. E., and Dyson, H. J. (2002) *Biochemistry 41*, 12681−12686.
62. Lietzow, M. A., Jamin, M., Dyson, H. J., and Wright, P. E. (2002) *J. Mol. Biol. 322*, 655−662.
63. Frauenfelder, H., Sligar, S. G., and Wolynes, P. G. (1991) *Science 254*, 1598−1603.
64. Glasoe, P. K., and Long, F. A. (1960) *J. Am. Chem. Soc. 64*, 188−190.
65. Konermann, L., Rosell, F. I., Mauk, A. G., and Douglas, D. J. (1997) *Biochemistry 36*, 6448−6454.
66. Zechel, D. L., Konermann, L., Withers, S. G., and Douglas, D. J. (1998) *Biochemistry 37*, 7664−7669.
67. Konermann, L. (1999) *J. Phys. Chem. A 103*, 7210−7216.
68. Collings, B. A., and Douglas, D. J. (1996) *J. Am. Chem. Soc. 118*, 4488−4489.
69. Hunter, C. H., Mauk, A. G., and Douglas, D. J. (1997) *Biochemistry 36*, 1018−1025.
70. Philo, J. S. (1996) *Biophys. J. 72*, 435−444.
71. Ralston, G. (1993) *Introduction to Analytical Ultracentrifugation*, Beckman Instruments, Inc., Fullerton, CA.
72. Cole, J. L., and Hansen, J. C. (1999) *J. Biomol. Technol. 10*, 163−176.
73. Lide, D. R. (2001) *CRC Handbook of Chemistry and Physics*, 82nd ed., CRC Press, London.
74. Hinz, H. J. (1986) *Thermodynamic Data for Biochemistry and Biotechnology*, Springer-Verlag, New York.
75. Katta, V., and Chait, B. T. (1991) *J. Am. Chem. Soc. 113*, 8534−8535.
76. Jamin, M., and Baldwin, R. L. (1998) *J. Mol. Biol. 276*, 491−504.
77. Fändrich, M., Fletcher, M. A., and Dobson, C. M. (2001) *Nature 410*, 165−166.
78. Eliezer, D., Chiba, K., Tsuruta, H., Doniach, S., Hodgson, K. O., and Kihara, H. (1993) *Biophys. J. 65*, 912−917.
79. Robinson, C. V., Chung, E. W., Kragelund, B. B., Knudsen, J., Aplin, R. T., Poulsen, F. M., and Dobson, C. M. (1996) *J. Am. Chem. Soc. 118*, 8646−8653.
80. Mauk, M. R., Mauk, A. G., Chen, Y.-L., and Douglas, D. J. (2002) *J. Am. Soc. Mass Spectrom. 13*, 59−71.
81. Hermans, J., J., Puett, D., and Acampora, G. (1969) *Biochemistry 8*, 22−30.
82. Clark, S. M., and Konermann, L. (2003) *J. Am. Soc. Mass Spectrom.* (submitted for publication).
83. Cech, N. B., and Enke, C. G. (2000) *Anal. Chem. 72*, 2717−2723.
84. March, R. E. (1997) *J. Mass Spectrom. 32*, 351−369.
85. Wuthrich, K. (1986) *NMR of Proteins and Nucleic Acids*, John Wiley and Sons, Toronto.
86. Miranker, A., Robinson, C. V., Radford, S. E., and Dobson, C. M. (1996) *FASEB J. 10*, 93−101.
87. La Mar, G. N., and Krishnamoorthi (1984) *J. Am. Chem. Soc. 106*, 6395−6401.
88. Aojula, H. S., Wilson, M. T., and Drake, A. (1986) *Biochem. J. 237*, 613−616.
89. Light, W. R., Rohlfs, R. J., Palmer, G., and Olson, J. (1987) *J. Biol. Chem. 262*, 46−52.
90. Chamberlain, A. K., Handel, T. M., and Marqusee, S. (1996) *Nat. Struct. Biol. 3*, 782−787.
91. Fuentes, E. J., and Wand, A. J. (1998) *Biochemistry 37*, 3687−3698.
92. Arrington, C. B., Teesch, L. M., and Robertson, A. D. (1999) *J. Mol. Biol. 285*, 1265−1275.
93. Bhuyan, A. K., and Udgaonkar, J. B. (1998) *Proteins: Struct., Funct., Genet. 30*, 295−308.
94. Barrick, D., and Baldwin, R. L. (1993) *Biochemistry 32*, 3790−3796.
95. Hargrove, M. S., Krzywda, S., Wilkinson, A., Dou, Y., Ikeda-Saito, M., and Olson, J. S. (1994) *Biochemistry 33*, 11767−11775.
96. Konermann, L., and Douglas, D. J. (1998) *Rapid Commun. Mass Spectrom. 12*, 435−442.
97. Woodward, C. (1993) *Trends Biochem. Sci. 18*, 359−360.
98. Fersht, A. (1999) *Structure and Mechanism in Protein Science*, W. H. Freeman, New York.
99. Kaltashov, I. A., and Eyles, S. J. (2002) *J. Mass. Spectrom. 37*, 557−565.
100. Döring, K., Surrey, S., Grunewald, S., John, E., and Jahnig, F. (2000) *Protein Sci. 9*, 2246−2250.

BI034285E